Comput Visual Sci (2010) 13:177–185
DOI 10.1007/s00791-010-0136-2

REGULAR ARTICLE

A multigrid finite element method for reaction-diffusion systems on surfaces

Christoph Landsberg · Axel Voigt

Received: 29 April 2009 / Accepted: 21 February 2010 / Published online: 22 April 2010
© Springer-Verlag 2010

Abstract We develop a multigrid finite element approach to solve PDE's on surfaces. The multigrid approach involves the same weights for restriction and prolongation as in the case of planar domains. Combined with the concept of parametric finite elements the approach thus allows to reuse code initially developed to solve problems on planar domains to solve the corresponding problem on surfaces. The method is tested on a non-linear reaction-diffusion system on stationary and evolving surfaces, with the normal velocity of the evolving surface depending on the reaction-diffusion system. As a reference model the Schnakenberg system is used, offering non-linearity and algebraic simplicity on one hand, and quantitative reference data on the other hand.

1 Introduction: PDE's on surfaces

Motivated by various applications especially in biology, materials science and image processing, there is a growing interest to solve PDE's on surfaces. While the solution of PDE's on Cartesian grids has become a standard tool the numerical solution of PDE's on surfaces is much less understood. Only recently various numerical methods have been proposed to solve a general class of PDE's on surfaces. They can be distinguished into direct methods, which require a surface mesh and indirect methods in which the surface is only implicitly described. Within the first approach parametric finite elements can be used to solve the PDE, see e.g. [1–4]. Level set method have been used within the second approach, see e.g. [5–8]. Furthermore also phase-field models can be used to implicitly describe the surface, as used in Ref. [9–11]. In order for the implicit approach to be efficient, adaptively refined meshes or narrow band approaches are required. For recent approaches in this direction see [12–15]. We will here concentrate on the direct approach of parametric finite elements and discuss a multigrid algorithm and results for a reaction-diffusion equation to model pattern formation on stationary and evolving surfaces.

The paper is organized as follows: In Sect. 2 we review the concept of parametric finite elements and show how available finite element code to solve problems on Cartesian grids can be used to solve also problems on triangulated surfaces. In Sect. 3 we discuss as a model problem on a surface a reaction-diffusion equation of Schnkenberg type on various stationary and evolving domains. We use a hierarchy of surfaces meshes and a multigrid solver. Finaly we draw conclusions in Sect. 4.

2 Using FEM to solve PDE's on triangulated surfaces

We consider the following PDE, which serves as a model problem and describes a general second order parabolic equation on a closed stationary surface $\Gamma \subset \mathbb{R}^d$, $d = 2, 3$, with $d = 2$ representing the case of a curve instead of a surface

$$u_t - \nabla_\Gamma \cdot A\nabla_\Gamma u + b \cdot \nabla_\Gamma u + cu = f \quad \text{on } \Gamma, \text{for } t > 0 \quad (1)$$

$$u(\cdot, 0) = u_0 \quad \text{on } \Gamma, \quad (2)$$

with problem specific parameters $A = A(u, \nabla_\Gamma u, \mathbf{x}, t)$, $b = b(u, \nabla_\Gamma u, \mathbf{x}, t)$ and $c = c(u, \nabla_\Gamma u, \mathbf{x}, t)$, with $\nabla_\Gamma \cdot$ and ∇_Γ the surface divergence and surface gradient, respectively, and $\mathbf{x} \in \Gamma$ and $t \in (0, T]$. The right hand side is given by $f = f(\mathbf{x}, t)$, while the initial condition is given by $u_0 = u_0(\mathbf{x})$. For all these functions we assume appropriate regularity. We further assume an existing representation of u off the sur-

C. Landsberg (✉) · A. Voigt
Institut für Wissenschaftliches Rechnen, Dresden, Germany
e-mail: christoph.landsberg@tu-dresden.de

A. Voigt
e-mail: axel.voigt@tu-dresden.de

face, to be able to formulate the spatial derivatives in $\mathbb{R}^d$. With $X = H^1(\Gamma)$ the weak form reads

$$\int_\Gamma u_t \phi \, d\Gamma + \int_\Gamma A \nabla_\Gamma u \cdot \nabla_\Gamma \phi \, d\Gamma + \int_\Gamma b \cdot \nabla_\Gamma u \phi \, d\Gamma + \int_\Gamma c u \phi \, d\Gamma = \int_\Gamma f \phi \, d\Gamma \tag{3}$$

for all $\phi \in X$. Now we split the time interval by discrete time instants $0 = t_0 < t_1 < \dots$ and define the time steps $\tau^n = t_{n+1} - t_n$. We consider at time instant t_n finite dimensional subspaces $X^n_{h,i} \subset X^n = H^1(\Gamma)$ with $N^n_i = dim\ X^n_{h,i}, i = 1, 2$ to allow for different spaces. For simplicity lets apply an implicit Euler discretization in time. The discrete solution of (3) is then given by: Find $u^{n+1}_h \in X^{n+1}_{h,1}$ such that

$$\int_\Gamma \frac{u^{n+1}_h - u^n_h}{\tau^n} \phi_h \, d\Gamma + \int_\Gamma A \nabla_\Gamma u^{n+1}_h \cdot \nabla_\Gamma \phi_h \, d\Gamma + \int_\Gamma b \cdot \nabla_\Gamma u^{n+1}_h \phi_h \, d\Gamma + \int_\Gamma c u^{n+1}_h \phi_h \, d\Gamma = \int_\Gamma f \phi_h \, d\Gamma \tag{4}$$

for all $\phi_h \in X^{n+1}_{h,2}$. If we treat all dependencies of the parameters on u explicitly, the resulting equation becomes linear. Now choosing basis $\{\phi_1, \dots, \phi_{N^n_1}\}$ and $\{\psi_1, \dots, \psi_{N^n_2}\}$ of $X^n_{h,1}$ and $X^n_{h,2}$, respectively. For $v^n_h \in X^n_{h,1}$ we denote by $V^n = (V^n_1, \dots, V^n_{N^n_1})$ the coefficient vector of v^n_h, with respect to the basis $\{\phi_1, \dots, \phi_{N^n_1}\}$, i.e.

$$v^n_h = \sum_{j=1}^{N^n_1} V^n_j \phi_j. \tag{5}$$

Using (4) with test functions $\psi_i, i = 1, \dots, N^{n+1}_2$, we get the following equations for the coefficient vector U^{n+1} of u^{n+1}_h

$$\frac{1}{\tau^n} \sum_{j=1}^{N^{n+1}} U^{n+1}_j \int_{\Gamma^{n+1}} \phi_j \psi_i \, d\Gamma + \sum_{j=1}^{N^{n+1}} U^{n+1}_j \times \int_{\Gamma^{n+1}} A \nabla_\Gamma \phi_j \cdot \nabla_\Gamma \psi_i \, d\Gamma + \sum_{j=1}^{N^{n+1}} U^{n+1}_j \times \int_{\Gamma^{n+1}} b \cdot \nabla_\Gamma \phi_j \psi_i \, d\Gamma + \sum_{j=1}^{N^{n+1}} U^{n+1}_j \int_{\Gamma^{n+1}} c \phi_j \psi_i \, d\Gamma = \int_\Gamma \tilde{f} \psi_i \, d\Gamma + \frac{1}{\tau^n} \sum_{j=1}^{N^n} U^n_j \int_\Gamma \phi_j \psi_i \, d\Gamma$$

for $i = 1, \dots, N^{n+1}_2$. The resulting system has to be assembled, which is done by looping over all grid elements and using quadrature formulas for each element to compute the integrals. If $\mathcal{T}^{n+1}$ is a surface triangulation of Γ^{n+1} with elements T^{n+1} the integrals read

$$\int_\Gamma \phi_j \psi_i \, d\Gamma = \sum_{T^{n+1} \in \mathcal{T}^{n+1}} \int_{T^{n+1}} \phi_j \psi_i \, d\Gamma, \quad \dots \tag{6}$$

where the sum can be restricted to $T^{n+1} \subset supp\ \phi_j \cap supp\ \psi_i$. Now instead of performing the integration on the surface elements T^{n+1}, a parameterization $F_T : \hat{T} \to T^{n+1}$ is used, with $\hat{T} = conv\, hull\, \{0, \mathbf{e}_1, \dots, \mathbf{e}_d\}$ the *standard element* in $\mathbb{R}^d$, with $d = 1, 2$. Furthermore the basis functions are defined on a *reference element* $\overline{T} = \{(\lambda_0, \dots, \lambda_d) \in \mathbb{R}^{d+1}; \lambda_k \geq 0, \sum_{k=0}^d \lambda_k = 1\}$ using barycentric coordinates. These allow to rewrite the integrals as

$$\int_{T^{n+1}} A \nabla_\Gamma \phi_j \cdot \nabla \psi_i \, d\Gamma = \int_{\hat{T}} \bar{A} \nabla_\lambda \phi_j(\lambda(\hat{\mathbf{x}})) \cdot \nabla_\lambda \psi_i(\lambda(\hat{\mathbf{x}})) \, d\hat{\mathbf{x}}$$

$$\int_{T^{n+1}} b \cdot \nabla_\Gamma \phi_j \psi_i \, d\Gamma = \int_{\hat{T}} \bar{b} \nabla_\lambda \phi_j(\lambda(\hat{\mathbf{x}})) \cdot \psi_i(\lambda(\hat{\mathbf{x}})) \, d\hat{\mathbf{x}}$$

$$\int_{T^{n+1}} c \phi_j \psi_i \, d\Gamma = \int_{\hat{T}} \bar{c} \phi_j(\lambda(\hat{\mathbf{x}})) \psi_i(\lambda(\hat{\mathbf{x}})) \, d\hat{\mathbf{x}}$$

and so on, with $\bar{A} = \Lambda(F_T(\hat{\mathbf{x}})) A \Lambda^t(F_T(\hat{\mathbf{x}})) |\det DF_T(\hat{\mathbf{x}})|$, $\bar{b} = \Lambda(F_T(\hat{\mathbf{x}})) b |\det DF_T(\hat{\mathbf{x}})|$, $\bar{c} = c |\det DF_T(\hat{\mathbf{x}})|$ and Λ the Jacobian of the barycentric coordinates on T^{n+1}. In this way we transform all integrations onto the *standard element* and have the definition of basis functions on the *reference element* at hand. Both are defined in $\mathbb{R}^d$ and $\mathbb{R}^{d+1}$. The parameterization F_T is given by the coordinates of the mesh elements and provides the only difference between solving equations on surfaces and on planar domains. For a surface we have to allow $F_T : \mathbb{R}^d \to \mathbb{R}^{d+1}$, whereas for a planar domain $F_T : \mathbb{R}^d \to \mathbb{R}^d$. With this tiny modification any code to solve PDE's on cartesian grids can be used to solve the same problem on a surface, providing a surface triangulation is given. Within an efficient implementation this does not even require to recompile a running 1D or 2D code, but only a change in a parameter file, as e.g. done in AMDiS [2]. With this approach all available tools to solve PDE's on planar domains, such as adaptive refinement or parallelization approaches, can be used also to solve PDE's on surfaces. We will demonstrate in the following that also multigrid solvers can be carried over. Analytic justification for these are however missing in many situations. One problem results from adaptive refinements on surface meshes, which require to project inserted grid points to the surface, see Fig. 1.

Thus coarser triangular surfaces do no longer generate a sequence of nested finite element spaces. As a consequence convergence results for multigrid solvers based on subspace

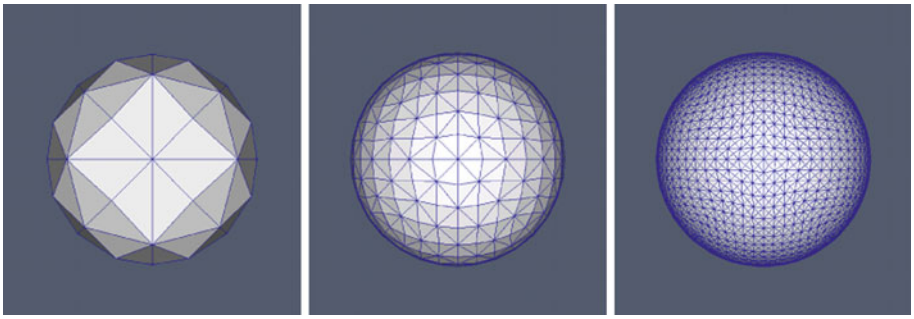

Fig. 1 Globally refined surface mesh. Refinement levels 3,6,9 (from *left* to *right*)

correction method can no longer be applied. We will not address this theoretical question but test a straightforward approach in which the same weights for restriction and prolongation as in the case of planar triangulations are used to solve a problem on a surface mesh. A similar approach have already been used to solve the Einstein equations [16] or for preconditioners [17] and a theoretical justification for the special case of an open surface was given in [18]. We apply the concept to solve reaction-diffusion equations on surfaces to model biological pattern formation.

3 Reaction-diffusion systems and biological pattern formation

Reaction-diffusion systems are prominent candidates for pattern generation mechanisms in various processes ranging from biological, chemical, and physical up to economical systems. We will here concentrate on biological applications. In morphogenesis of living organisms, positional information and prepatterning processes are required in order to guide developmental processes and the building-up of higher order structures. Other pattern formation processes observed in biological systems concern the coat patterning of animals. During the coarse of evolution, different mechanisms of pattern formation may have developed, which differ in function, but may be based on some basic patterning mechanisms. Turing proposed a theory of morphogenesis based on interacting and diffusing molecules which he called morphogens, meaning that they are suggested to contribute to the formation of the body of living organisms [19]. In the context of reaction-diffusion systems, an inhomogenous spatial pattern of the interacting molecules arises if the diffusion constants of at least two reactive species is different to each other, while feedback loops are involved in determing the nonlinear kinetics of the system. This concept is commonly denoted as Turing system, and the instability leading to pattern formation is called Turing instability. Different kinetics and models have emerged over the past decades, see e.g. [20–22]. We focus on the Schnakenberg system, as it is one of the best studied and algebraically most simple non-linear reaction diffusion system, thus being a suitable model to test the effectiveness of the multigrid solver.

3.1 The Schnakenberg model

The Schnakenberg model [22] describes the interaction of a long range inhibitor with a short range autocatalyst, also called activator, in a tri-molecular interaction. The model reaction steps can be summarised with the following system of chemical reaction equations,

$$X \rightleftharpoons A, \qquad B \to Y, \qquad 2X + Y \to 3X.$$

The functional description of the corresponding reaction kinetics reads

$$f(u, v) = a - u + u^2 v \tag{7}$$
$$g(u, v) = b - u^2 v, \tag{8}$$

where u and v correspond to the non-dimensionalized concentrations X and Y, respectively. The Schnakenberg system can now be formulated in general as a system of parabolic partial differential equations on an evolving surface $\Gamma = \Gamma(t)$:

$$\partial_t u = \Delta_\Gamma u + \gamma f(u, v) \tag{9}$$
$$\partial_t v = d\Delta_\Gamma v + \gamma g(u, v). \tag{10}$$

The parameter d constitutes the ratio of the diffusion coefficients of D_v and D_u and is an essential parameter influencing the range of parameters for which Turing patterns are predicted to form, see [23]. The parameter γ models the strength of the chemical reaction.

3.2 Discretization

Let $\phi \in V \subset H^1(\Gamma)$ be a test function, and $\int_\Gamma \cdot \phi \, d\Gamma = (\cdot, \phi)$ be the L_2 inner product. The general Schnakenberg model equations can then be described in the weak form

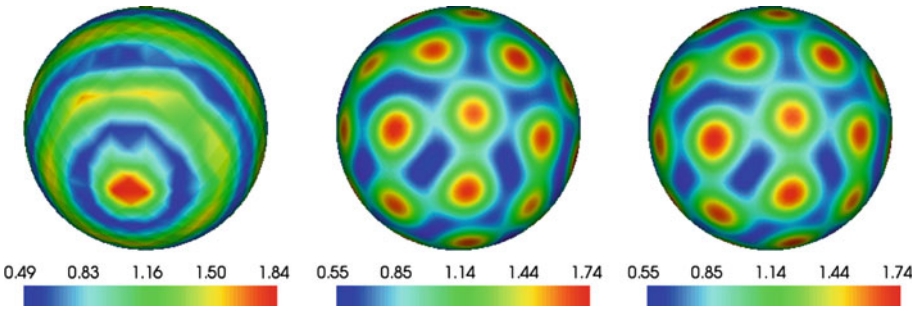

Fig. 2 Schnakenberg pattern on a sphere of radius $r = 1/\sqrt{(4\pi)}$ for grid constants $h = (0.035, 0.0175, 0.00875)$ corresponding to global refinement levels 7, 9, and 11, respectively, applied to our initial coarse grid

$$(\partial_t u, \phi) + (\nabla_\Gamma u, \nabla_\Gamma \phi) + (\gamma u, \phi) - \left(\gamma u^2 v, \phi\right) = (\gamma a, \phi) \tag{11}$$

$$(\partial_t v, \phi) + (d\nabla_\Gamma v, \nabla_\Gamma \phi) + \left(\gamma u^2 v, \phi\right) = (\gamma b, \phi)\,. \tag{12}$$

We use a semi-implicit discretization scheme suggested in [24] for this system. Using linear finite elements $\phi_h \in V_h$, with $V_h \subset V$ a finite dimensional subspace, the fully-discrete general Schnakenberg system can be formulated as

$$\begin{aligned}
&\left(\frac{u_h^{n+1} - u_h^n}{\tau^n}, \phi_h\right) + \left(\nabla_\Gamma u_h^{n+1}, \nabla_\Gamma \phi_h\right) + \left(\gamma u_h^{n+1}, \phi_h\right) \\
&\qquad - \left(\gamma u_h^n v_h^n u_h^{n+1}, \phi_h\right) = (\gamma a, \phi_h) \\
&\left(\frac{v_h^{n+1} - v_h^n}{\tau^n}, \phi_h\right) + \left(d\nabla_\Gamma v_h^{n+1}, \nabla_\Gamma \phi_h\right) \\
&\qquad + \left(\gamma u_h^n u_h^n v_h^{n+1}, \phi_h\right) = (\gamma b, \phi_h)\,,
\end{aligned}$$

where $\tau^n = t^{n+1} - t^n$. Due to the semi-implicit discretization the resulting equations are linear. In order to formulate the discretized Schnakenberg system as a linear system of equations in matrix notation, we employ the coefficient vectors U^{n+1} and V^{n+1}, i.e.$u_h^{n+1} = \sum U_i^{n+1}\phi_i$ and $v_h^{n+1} = \sum V_i^{n+1}\phi_i$. Furthermore, for the assembling of the system matrix, we define:

$$\begin{aligned}
&M = \left(M_{ij}\right), M_{ij} = \left(\phi_i, \phi_j\right);\\
&A = \left(A_{ij}\right), A_{ij} = \left(\nabla_\Gamma \phi_i, \nabla_\Gamma \phi_j\right);\\
&R_a = \left(R_{a,i}\right), R_{a,i} = (a, \phi_i);\\
&R_b = \left(R_{b,i}\right), R_{b,i} = (b, \phi_i);\\
&F_{uv} = \left(F_{uv,ij}\right), F_{uv,ij} = \left(u_h^n v_h^n \phi_i, \phi_j\right);\\
&F_{u^2} = \left(F_{u^2,ij}\right), F_{u^2,ij} = \left(u_h^n u_h^n \phi_i, \phi_j\right),
\end{aligned}$$

where A and M being the stiffness and mass matrices, respectively, R_a and R_b are the remaining right-hand-side operators, while F_{uv} and F_{u^2} are the matricies representing the linearization of the non-linear Schnakenberg reaction kinetics. Using these notations the discretized Schnakenberg model reads:

$$\begin{aligned}
&\frac{1}{\tau^n} M U^{n+1} + \gamma U^{n+1} + A U^{n+1} - \gamma F_{uv} U^{n+1} \\
&\quad = \frac{1}{\tau^n} M U^n + \gamma R_a \frac{1}{\tau^n} M V^{n+1} + dA V^{n+1} \\
&\qquad + \gamma F_{u^2} V^{n+1} = \frac{1}{\tau^n} M V^n + \gamma R_b.
\end{aligned}$$

The system matrix can now be assembled as

$$\begin{pmatrix} \frac{1}{\tau^n} M + \gamma M + A - \gamma F_{uv} & 0 \\ 0 & \frac{1}{\tau^n} M + dA + \gamma F_{u^2} \end{pmatrix} \begin{pmatrix} U^{n+1} \\ V^{n+1} \end{pmatrix} = \begin{pmatrix} \frac{1}{\tau^n} M U^n + \gamma R_a \\ \frac{1}{\tau^n} M V^n + \gamma R_b \end{pmatrix}.$$

The linear system is solved using a standard multigrid solver.

3.3 Grid independence

We start by showing grid independence of the solution on a sphere with surface area of $Area = 1$. The solutions are calculated with the multigrid solver, see Fig. 2. Qualitative differences in pattern morphology are observable. for refinement levels $L < 9$, where the regular spot pattern breaks down, whereas it remains stable for $L \geq 9$. These observations suggest a grid constant of $h = 0.0175$, corresponding to 9 global refinements, to be applied to the initial coarse grid. This has been carried out for all further numerical calculations.

3.4 Results on a spherical domain

Various numerical approach have been used to solve such systems on spherical domains, see e.g. [25–30]. Most of these approaches are restricted to the special structure of a sphere. Our approach can be used on any surface, we just require a hierarchy of refined surface triangulations. However, such a hierachy might not be available for general surfaces. In many applications it will be much more common to have a geometry described only by a fine mesh available, which might result from range scanning techniques, see e.g. [31]. We thus must address the issue of mesh coarsening, which is related to mesh simplification, commonly used in computer graphics. For a review on available approaches see e.g. [17].

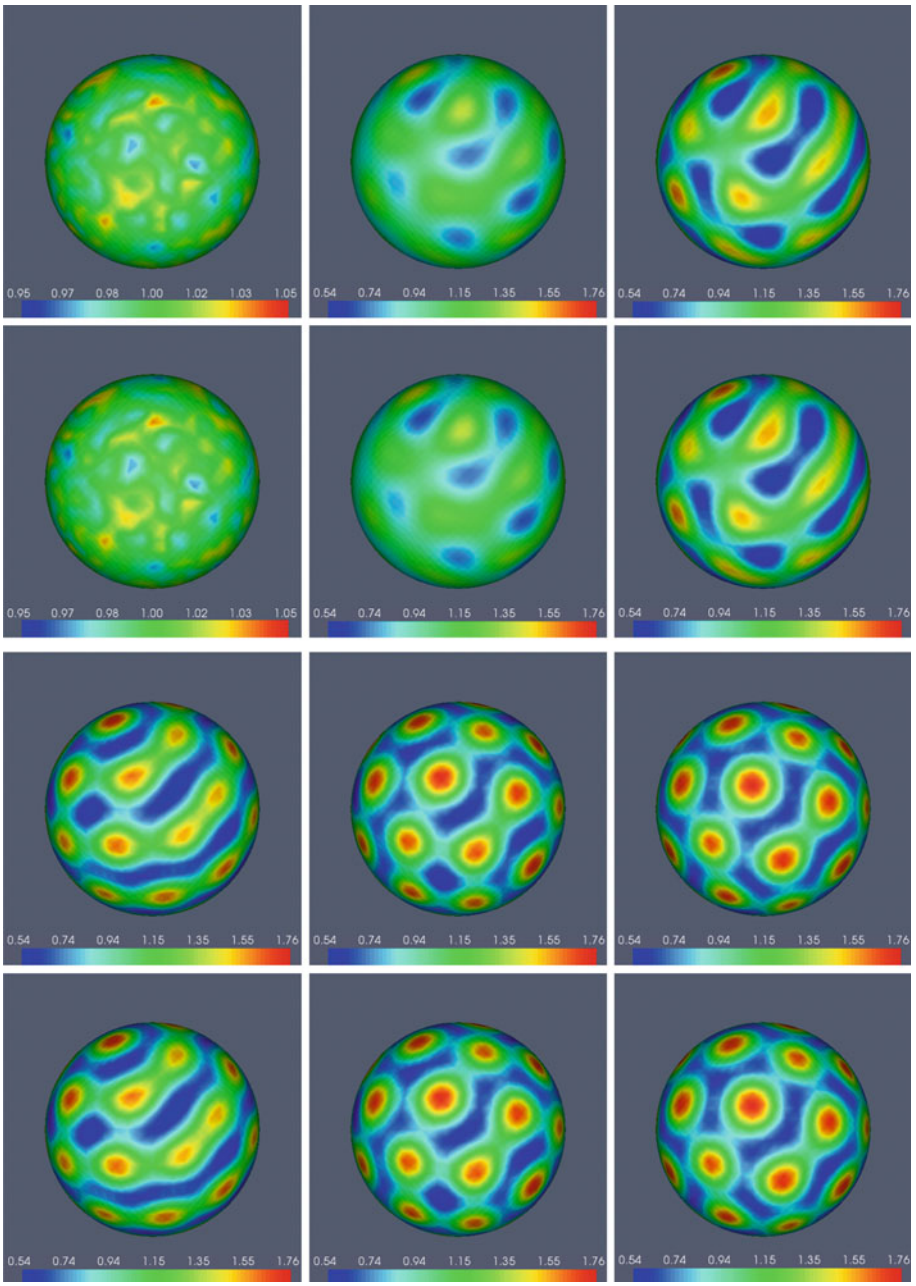

Fig. 3 Concentrations for the Schnakenberg model on a sphere. Parameters: $a = 0.1$, $b = 0.9$, $u_s = 1.0$, $v_s = 0.9$, $d = D_v/D_u = 10.0$, $\gamma = 5000$. A total of 2113 gridpoints has been used to define 4,096 triangular elements. Time is discretized with $\tau = 0.00001s$. Pairs **a:d**, **b:e**, **c:f**, **g:j**, **h:k**, **i:l** (**a–l** numerated from *top left* to *bottom right*) depict the solutions of BiCGStab:multigrid at corresponding time points of 0.0091, 0.0191, 0.0291, 0.1091, 0.2091 s and 5.0 s, respectively

We first compare results on a sphere obtained with the multigrid and a BiCGStab solver. Several representative times have been chosen in order to give an impression about the time development of the pattern evolution, as well as to check if the intermediate solutions obtained with both solvers are identical. Figure 3 shows both results for various times and indicates the agreement of both results.

Figure 4 shows the solution for different refinement levels, i.e. on the different levels of multigrid. Due to the projection, the refinements at different levels correspond to practically different domains. However, the domain adaptivity seems to have no influence on the multigrid solver. The more refinements are carried out, the better is the approximation of the sphere.

3.5 Stability issues with respect to size and perturbations of the domain

We now apply the approach to solve the reaction-diffusion system on modified domains. We first vary only the radius

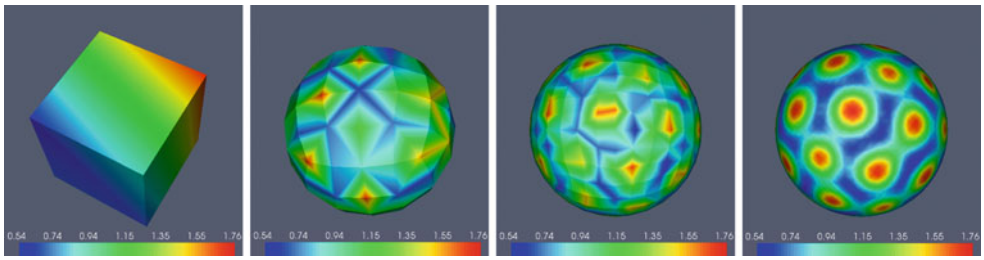

Fig. 4 Example levels from the multigrid solver at global refinement levels 0, 4, 6, and 9 (from *left* to *right*)

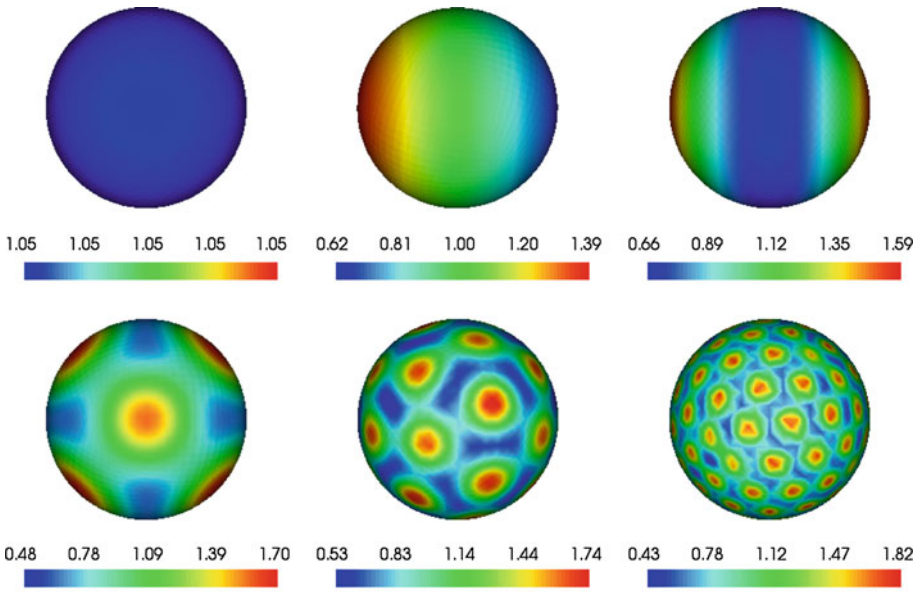

Fig. 5 Multigrid solutions for the Schnakenberg model for different radii $r = 0.15625$, 0.03125, 0.0625, 0.125, 0.25, 0.5 and parameters as before ($b = 0.9$, $u_s = 1.0$, $v_s = 0.9$, $d = D_v/D_u = 10.0$, $\gamma = 5000$), evaluated at time $t = 20.0$ s

of the sphere and numerically obtain a dependence of the stability region and formed pattern on size (see Fig. 5 for the dependence on the forming patterns on the radius). We observe an increase of the number of spots of high activator concentration for increasing radius, which is consistent with other numerical results adressing the influence of the domain size, e.g.[24,30] and linear stability results in e.g. [28].

In the next step we modify our domain and solve the reaction-diffusion system on a perturbed sphere. As a perturbation we use spherical harmonics (see Fig. 6 for the corresponding results).

For the perturbed sphere we observe spot-like regions of high activator concentrations located near the highest curvature regions of the domain. However, this effect seems to be overlayed by the tendency of the spots to distribute over the whole size of the domain, which is a consequence of the action of the long range inhibitor, limiting the spreading of islands of self-enhancing activators, and is valid for both the unperturbed and perturbed sphere. Furthermore, both the perturbed and the unperturbed sphere share the influence of size on the number and relative position of spots. Remarkably, the changed geometries of the perturbed spheres seem to induce a distortion of the angles within triangles of spots (as for instance in the second row, first and second panel of Fig. 6), which has direct consequences on the spot morphologies observed. On both of these disturbed spheres, spots are positioned close to or exactly on an imaginative circle. As a consequence, their relative distances along those circles are small, whereas spots in the opposite direction are further away, being in less contact or even being seperated from their neighbors. The separation of spots is an effect of the increased surface area of the perturbed spheres, but the distorted angles between spot–spot axes, which are isotropic far away from the ideal case of 60 degrees is clearly visible for all depicted variants of perturbed spheres, although this effect is weakened for the Y_2^1-based and Y_3^1-based perturbation. We argue that in contrast to the other perturbed spheres, the distribution and number of localized regions of high curvature enables the spots to distribute evenly enough to avoid close proximity of spots, resulting in a relatively lowered intensity of spot fusion. A meaningful example reflecting such effects in nature could be the embryonic development of skin pigmentation prepatterns (cf. [23,32] for details), as differences in the curvature of the body, as found for instance at the

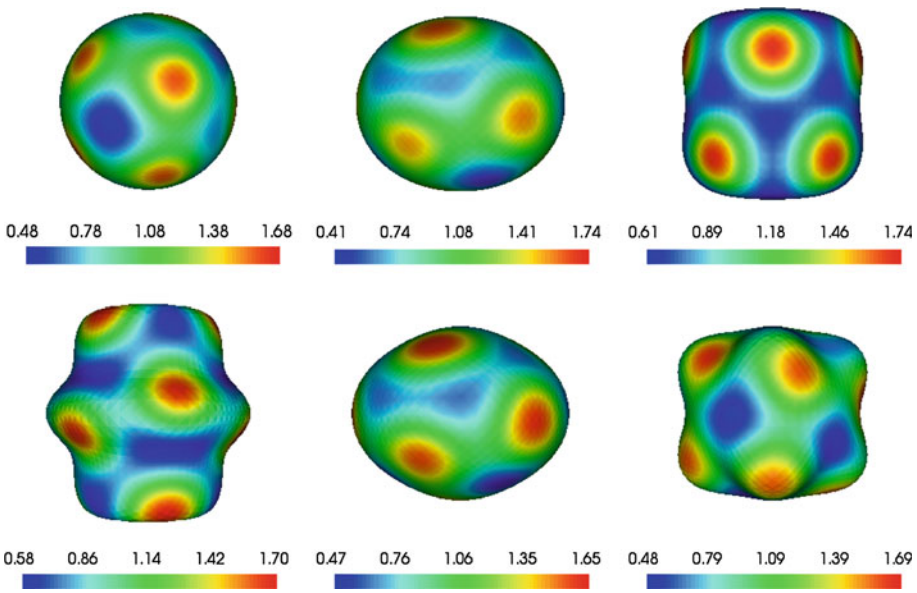

Fig. 6 Schnakenberg pattern on an undisturbed and disturbed sphere with initial radius of $r = 0.125$, evaluated at time $t = 20.0$ s. Starting from the second panel, the initial spherical coordinates, as applied in the first panel, have been superposed with damped absolute values of squared real parts of spherical harmonics $Y_1^1, Y_2^1, Y_3^1, Y_2^2, Y_2^3$, respectively, using a factor of 0.2 for damping of the amplitudes of $abs\left(Re^2(Y_l^m)\right)$. Model parameters have been chosen as before

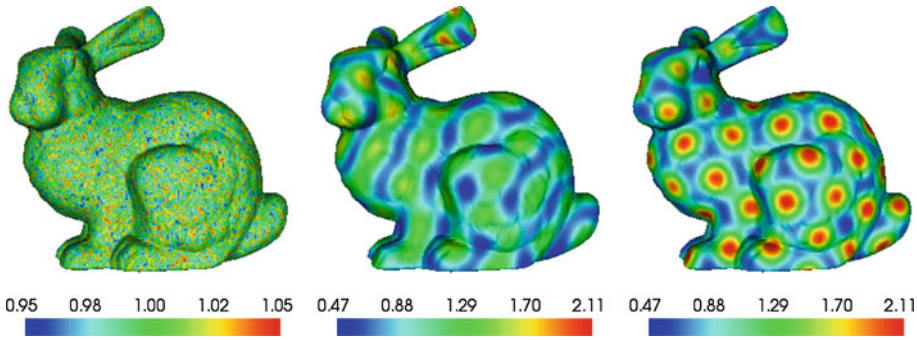

Fig. 7 Schnakenberg pattern on the surface of the Stanford bunny after $t = 0.00, 0.05$, and 10 s respectively. Model parameters have been chosen as before

periphery of the body, are leading to different morphologies of patterns or fusion of close spots to stripes, for instance regarding the tail patterns of Leopards (cf. [33]). The directionality of the observed fusing spots could be an effect of curvature-induced anisotropy as observed for the disturbed spheres. The influence of such anisotropies is described in [34], which is consistent with our findings. Nevertheless it is not clear to which extend these anisotropies are induced by curvature in relation to the randomly induced anisotropies created by noisy initial activator and inhibitor concentrations.

As a final example for the pattern formation on fixed domains we solve the reaction-diffusion system on the Stanford bunny as a more complicated example.

In Fig. 7 it is shown that after a transition phase in which stripe patterns may arise, the predominating patterns, as with most examples shown here, are spots. In contrast to the sphere, both the disturbed sphere and the Stanford bunny show increased pattern variability due to oscillation-like flow of concentration towards and away from regions of high curvature radii. Depending on the local morphology, the spots or stripes move according to the spacing of spots. If high activator concentrations come close together, the respective spots fuse and tend to create stripes. If larger regions of low activator concentration form, large neigboring spots tend to split or extend into the direction of lowest activator concentration. For the Stanford bunny the spot generation is fast in comparison to the sphere, but the rearrangement of spots is taking longer. The development of the pattern over time shows a high preference of stripe patterns to occur at an early stage of pattern development, remaining the predominant pattern for quite a while, which is consistent with the anisotropy conjecture formulated in the previous example. However, the last panel of Fig. 7 suggests that anisotropy is finally resolved at these locations, probably because of dilution effects and an increased average spot-to-spot distance after the folding-like movement and rupture of stripe patterns into individual spots of high activator concentrations. This behaviour seemingly contradicts the phenomena observed in biological systems, where stripe patterns at extremities remain stable over time. One possible explanation for this difference could be a switch-like resistance of the natural pattern to changes, once a certain activator or inhibitor concentration has been reached.

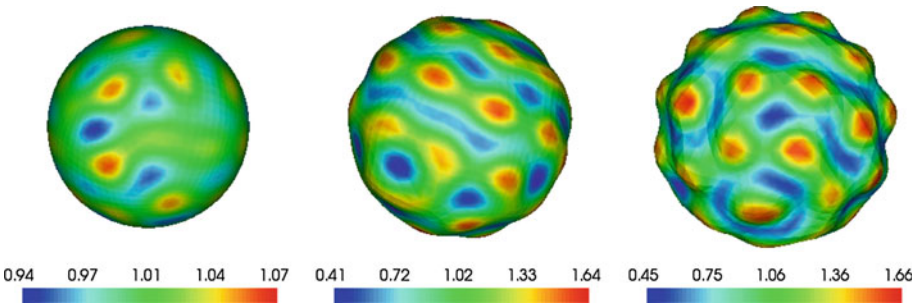

Fig. 8 Schnakenberg pattern after activator concentration-dependent growth in normal direction for $t = 0.00501, 0.03001$, and 0.05 s, respectively. Model parameters have been chosen as before

3.6 Evolving domain

We now want to consider pattern formation on a growing surface. We therefore define V the normal velocity of the surface as a function of activator species u, in the simplest case $V = cu$, with c a positive constant. The velocity vector $\vec{V} = Vn$ with n the surface normal can be computed as described in [35–37] by solving

$$\vec{\mathbf{M}}\,\vec{V} = \vec{\mathbf{N}}\,V, \tag{13}$$

where $\vec{\mathbf{M}}$ is a diagonal matrix with mass matrices $\mathbf{M} = (M_{ij}) = (\psi_i, \psi_j)$ as entries and $\vec{\mathbf{N}}$ is a vector of normal matrices $\left(N^k_{ij}\right) = (\psi_i, \psi_j n_k), i, j, k = 1, 2, 3$ with weights $n_k = \vec{n} \cdot \vec{e}_k$ containing the k-th spatial components of the normal. The vertex coordinates of the surface mesh are updated at the end of the m-th timestep τ_m as follows:

$$\vec{X} \to \vec{X} + \tau_m \vec{V}, \tag{14}$$

where $\vec{X}$ contains the spatial components of the vertex coordinates.

The surface coordinates are updated with linear growth with $c = 1.0001$ in normal direction, weighted with the surface concentrations of u at each vertex of the underlying mesh (results are shown in Fig. 8). This approach can only be viewed as an approximation in the case of a seperation of time scales between diffusion and surface evolution, with the diffusion being much faster, which is the most relevant case in many biological systems. In the more general case, where such a separation of time scales is not possible, the set of equations has to be modified to

$$\partial_t u - uVH = \Delta_\Gamma u + \gamma f(u, v) \tag{15}$$

$$\partial_t v - vVH = d\Delta_\Gamma v + \gamma g(u, v), \tag{16}$$

with H the mean curvature of the surface. Within this formulation we assume a constant extension of u and v in normal direction. All described numerical aspects can be extended to this and also more general cases in which also tangential velocities are allowed, see [1] for details.

We observe a preference of the activator u to reside in the exposed regions (i.e. where local growth enhancement has taken place before). This reflects the expected growth promotion of the activator due to local overweighting of the linear growth.

A similar concept of prepattern-dependent growth has already been applied in theoretical biology to model solid tumor growth (c.f. [28]). In this context, a basic growth of the tumor is enhanced locally in the direction of the highest concentration of growth factor molecules. The resulting protrusions are thought to be formed by solid tumors at the onset of malignancy, at a time when the ability of the cells to stop their growth upon the contact with cells from neighboring tissues is lost, and metastases may arise. An other example for concentration-dependent growth may be the positioning of hair follices or feathers in mice and chicken, respectively. In these cases, a prepattern of localized Wnt or Dkk molecules seems to induce a protrusion-like growth of hair follicle buds or feather buds in the direction of a local hot spot of concentration of one of the involved signaling molecules (see [38] and [39] for details). It is unclear which localized molecule concentrations are the cause and which the effect of these patterning mechanisms, but it seems likely that some isoforms of Wnt and Dkk may play the role of activators and inhibitors, leading to a prepatterned tissue.

4 Conclusions

We have reviewed the concept of parametric finite elements to solve PDE's on surfaces and pointed out that only a tiny modification is needed in standard finite element code to solve PDE's on cartesian grids to solve the corresponding PDE's on a surface mesh. The only requirement is to allow the mapping from a *standard element* to the mesh elements given through the parameterization $F_T : \hat{T} \to T^{n+1}$ to be a mapping from $\mathbb{R}^2$ to $\mathbb{R}^3$. Within an efficient implementation this does only require a change in a parameter file, as e.g. done in AMDiS [2]. With this approach all available tools to solve PDE's on planar domains, such as adaptive refinement, parallelization approaches, or multigrid solvers can be used also to solve PDE's on surfaces. We demonstrate the applicability of such a surface multigrid approach on a reaction diffusion system to model Turing patterns. Various examples are provided on different stationary and evolving domains demonstrating the flexibility and efficiency of the approach. However, the

usage of parametric finite elements in the context of evolving domains is not always possible. Difficulties arise once the surface undergoes topological changes for which tracking of the surface becomes a major issues which limit this approach. One alternative approach to circumvent these problems is to use an implicity description of the surface. A diffuse interface approach which in addition is coupled to a reaction diffusion equation in the bulk is described in [40].

Acknowledgments We would like to thank J. Lowengrub, F. Hausser and A. Madzvamuse for fruitful discussions. The work has been supported by DFG through Vo899/6-1.

References

1. Dziuk, G., Elliot, C.: Finite elements on evolving surfaces. IMA J. Num. Anal. **27**(2), 262–292 (2007)
2. Vey, S., Voigt, A.: Amdis: adaptive multidimensional simulations. Com. Vis. Sci. **10**, 57–67 (2007)
3. Dziuk, G., Elliot, C.M.: Surface finite elements for parabolic equations. J. Comput. Math. **25**(4), 385–407 (2007)
4. Stöcker, C., Voigt, A.: Geodesic evolution laws—a level set approach. SIAM J. Imag. Sci. **1**(4), 379–399 (2008)
5. Bertalmio, M., Cheng, L., Osher, S., Sapiro, G.: Variational problems and partial differential equations on implicit surfaces. J. Comput. Phys. **174**(2), 759–780 (2001)
6. Greer, B., Bertozzi, A., Sapiro, G.: Fourth order partial differential equations on general geometries. J. Comput. Phys. **216**(1), 216–246 (2006)
7. Dziuk, G., Elliot, C.M.: Eulerian finite element method for parabolic pdes on implicit surfaces. Interf. Free Boundaries **10**(1), 119–138 (2008)
8. Stöcker, C., Voigt, A.: A level set approach to anisotropic surface evolution with free adatoms. SIAM J. Appl. Math. **69**(1), 64–80 (2008)
9. Rätz, A., Voigt, A.: Pde's on surfaces—a diffuse interface approach. Commun. Math. Sci. **4**, 575–590 (2006)
10. Rätz, A., Voigt, A.: A diffuse-interface approximation for surface diffusion including adatoms. Nonlinearity **20**, 575–590 (2007)
11. Lowengrub, J., Rätz, A., Voigt, A.: Phase field modeling of the dynamics of multicomponent vesicles: spinodal decomposition, coarsening, budding, and fission. Phys. Rev. E **79**(3), 031,926 (2009)
12. Schwartz, P., Adalsteinsson, D., Coletta, P., Arkin, A., Onsum, M.: Numerical computation of diffusion on a surface. Proc. Nat. Acad. Sci. USA **102**(32), 11151–11156 (2005)
13. Ruuth, S., Merriman, B.: A simple embedding method for solving partial differential equations on surfaces. J. Comput. Phys. **227**, 1943–1961 (2008)
14. Elliott, C., Stinner, B.: Analysis of a diffuse interface approach to an advection diffusion equation on a moving surface. Math. Meth. Appl. Sci. p. to appear (2009)
15. Nemitz, O., Nielson, M., Rumpf, M., Whitaker, R.: Finite element methods for very large, dynamic tubular grid encoded implicit surfaces. SIAM J. Sci. Comput. **31**, 2259–2281 (2009)
16. Holst, M.: Adaptive numerical treatment of elliptic systems on manifolds. Adv. Comput. Math. **15**(14), 139–191 (2001)
17. Aksoylu, B., Khodakovsky, A., Schröder, P.: Multilevel solvers for unstructured surface meshes. SIAM J. Sci. Comput. **26**(4), 1146–1165 (2005)
18. Kornhuber, R., Yserentant, H.: Multigrid methods for discrete elliptic problems on triangular surfaces. Comput. Vis. Sci. **11**(4-6), 251–257 (2008)
19. Turing, A.M.: The chemical basis of morphogenesis. Phil. Trans. Roy. Soc. London B **237**, 37–72 (1952)
20. Gierer, A., Meinhardt, H.: A theory of biological pattern formation. Kybernetik **12**(1), 30–39 (1972)
21. Gray, P., Scott, S.K.: Autocatalytic reactions in the isothermal, continuous stirred tank reactor. isolas and other forms of multistability. Chem. Eng. Sci. **38**(1), 29–43 (1983)
22. Schnakenberg, J.: Simple chemical reaction systems with limit cycle behaviour. J. Theor. Biol. **81**(3), 389–400 (1979)
23. Murray, J. (ed.): Mathematical Biology (1989)
24. Madzvamuse, A.: Time-stepping schemes for moving grid finite elements applied to reaction-diffusion systems on fixed and growing domains. J. Comput. Phys. **214**(1), 239–263 (2006)
25. Gomatam, J., Amdjadi, F.: Reaction-diffusion equations on a sphere: meandering of spiral waves. Phys. Rev. E **56**, 3913–3919 (1997)
26. Varea, C., Aragon, J.L., Barrio, R.A.: Turing patterns on a sphere. Phys. Rev. E **60**(4), 4588–4592 (1999)
27. Yagisita, H., Mimura, M., Yamada, M.: Spiral wave behaviors in an excitable reaction–diffusion system on a sphere. Physica D **124** (1-3), 126–136 (1998)
28. Chaplain, M., Ganesh, M., Graham, I.: Spatio-temporal pattern formation on spherical surfaces: numerical simulation and application to solid tumour growth. J. Math. Bio. **42**(5), 387–423 (2001)
29. Pudykiewicz, J.A.: Numerical solution of the reaction–advection–diffusion equation on the sphere. J. Comput. Phys. **213**(1), 358–390 (2006)
30. Gjorgjeva, J., Jacobsen, J.: Turing patterns on growing spheres: the exponential case. Dis. Cont. Dyn. Sys., Supp. pp. 436–445 (2007)
31. Levoy, M., Rusinkiewicz, S., Ginzton, M., Ginsberg, J., Pulli, K., Koller, D., Anderson, S., Shade, J., Pereira, L., Davis, J., Fulk, D.: The digital michelangelo project: 3d scanning of large statues. In: SIGGRAPH 2000 Proceedings, pp. 131–144 (2000)
32. Kondo, S., Shirota, H.: Theoretical analysis of mechanisms that generate the pigmentation pattern of animals. Semin. Cell. Dev. Biol. **20**(1), 82–89 (2009)
33. Murray, J.: How the leopard gets its spots. Sci. Am. **258**(3), 80–87 (1988)
34. Shoji, H., Mochizuki, A., Iwasa, Y., Hirata, M., Watanabe, T., Hioki, S., Kondo, S.: Origin of directionality in the fish stripe pattern. Devel. Dyn. **226**(4), 627–633 (2003)
35. Bänsch, E., Haußer, F., Lakkis, O., Li, B., Voigt, A.: Finite element method for epitaxial growth with attachment–detachment kinetics J. Comput. Phys. **194**(2), 409–434 (2004)
36. Bänsch, E., Morin, P., Nochetto, R.: A finite element method for surface diffusion: the parametric case. J. Comput. Phys. **203**(1), 321–343 (2005)
37. Haußer, F., Voigt, A.: A discrete scheme for parametric anisotropic surface diffusion. J. Sci. Comput. **30**(2), 223–235 (2007)
38. Sick, S., Reinker, S., Timmer, J., Schlake, T.: WNT and DKK determine hair follicle spacing through a reaction-diffusion mechanism. Science **314**(5804), 1447–1450 (2006)
39. Yu, M., Wu, P., Widelitz, R., Chuong, C.: The morphogenesis of feathers. Nature **420**(6913), 308–312 (2002)
40. Li, X.J.L., Rätz, A.A.V.: Solving PDEs in complex geometries: a diffuse domain approach. Commun. Math. Sci. **7**(1), 81–107 (2009)